Jurnal Teknologi

Full Paper

CFD SIMULATION AND VALIDATION FOR MIXING VENTILATION SCALED-DOWN EMPTY AIRCRAFT CABIN USING OPENFOAM

Shahliza Azreen Sarmin[a,b], Azli Abd Razak[b], Fauziah Jerai[b*], Mohd Khir Harun[a]

[a]Malaysian Institute of Aviation Technology, Universiti Kuala Lumpur, 43800 Dengkil, Selangor, Malaysia
[b]School of Mechanical Engineering, College of Engineering, Universiti Teknologi MARA, 40450 Shah Alam, Selangor, Malaysia

Article history
Received
27 October 2022
Received in revised form
20 April 2023
Accepted
19 June 2023
Published Online
21 August 2023

*Corresponding author
fauziahjerai@uitm.edu.my

Graphical abstract

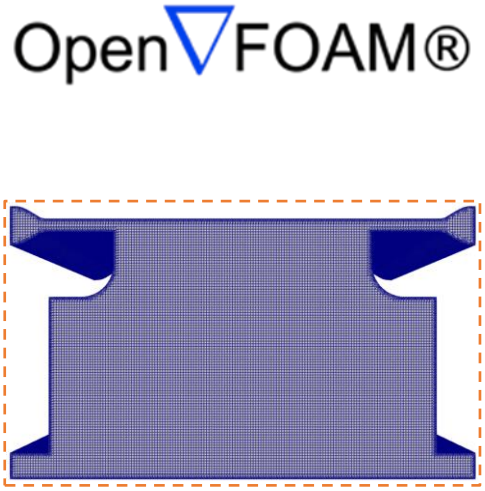

Abstract

An investigation into the spread of the COVID-19 virus within a confined space including an aircraft cabin is essential in order to find out the mechanism. However, this is time-consuming and limited in scope, so a computational fluid dynamics (CFD) simulation is used instead. Therefore, a prior study and an appropriate choice of turbulence model are required before the simulation. The main objective of this study is to validate and evaluate the results predicted by the Open Source Field Operation and Manipulation (OpenFOAM) software through comparison with the experimental data from the literature which was conducted using particle image velocimetry (PIV) measurement. Three different Reynolds-averaged Navier-Stokes turbulence models were selected; Re-normalisation Group k - ε (RNG), Realizable k - ε (RLZ) and Low Reynold Number (LRN) to simulate a mixing ventilation system of a scaled-down model of empty aircraft cabin. In the RNG and LRN model cases, a fairly large circulation flows were observed on the right and left sides of the model representing the passenger area. The results were also evaluated quantitatively using the factor of two of observations (FAC2) for the velocity components and turbulent kinetic energy (TKE) with root mean square error (RMSE) for the former and normalised mean square errors (NMSE) for the latter. The simulation results showed that RNG and LRN are capable of predicting the flow field well. However, for TKE prediction, LRN performed better than RNG which concluded that LRN is the suitable turbulence model in simulating flow fields in the investigated case.

Keywords: CFD, OpenFOAM, aircraft cabin, mixing ventilation, validation

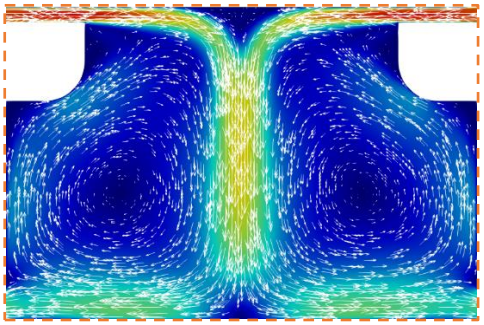

Abstrak

Penyiasatan terhadap penyebaran virus COVID-19 dalam ruang terkurung termasuk kabin pesawat adalah penting untuk mengetahui mekanisme itu. Walau bagaimanapun, ini memakan masa dan skopnya juga terhad. Oleh itu simulasi Computational Fluid Dynamic (CFD) digunakan. Kajian terdahulu dan pilihan model turbulensi yang sesuai perlu dilakukan sebelum simulasi dijalankan. Objektif utama kajian ini adalah untuk mengesahkan dan menilai keputusan yang diramalkan daripada perisian Open Source Field Operation and Manipulation (OpenFOAM) melalui perbandingan dengan data eksperimen daripada literatur yang telah dijalankan menggunakan velosimeter imej zarah (PIV). Tiga model pergolakan Reynolds-averaged Navier-Stokes yang berbeza; Re-normalisation Group k - ε (RNG), Realizable k - ε (RLZ) dan Low Reynold Number (LRN) dipilih untuk mensimulasikan sistem

pengudaraan campuran model kabin pesawat kosong berskala kecil. Dalam kes model RNG dan LRN, aliran pusaran yang agak besar diperhatikan di sebelah kanan dan kiri model yang mewakili kawasan penumpang. Hasilnya juga dinilai secara kuantitatif menggunakan factor two of observations (FAC2) untuk komponen halaju dan tenaga kinetik turbulen (TKE). Manakala purata ralat punca kuasa dua (RMSE) digunakan untuk komponen halaju dan normalised mean square errors (NMSE) untuk TKE. Keputusan simulasi menunjukkan bahawa RNG dan LRN mampu meramal medan aliran dengan baik. Walau bagaimanapun, model LRN adalah lebih baik daripada RNG untuk ramalan TKE. Oleh itu, dapat disimpulkan bahawa LRN adalah model turbulensi yang sesuai dalam mensimulasikan medan aliran dalam kes ini.

Kata kunci: CFD, OpenFOAM, kabin pesawat, pengudaraan campuran, pengesahan

1.0 INTRODUCTION

In commercial aircraft, the cabin ventilation system is crucial for the health and comfort of passengers and crew. Although the ventilation systems vary by aircraft type and manufacturer, most use mixing ventilation system. The mixing ventilation system delivers air from the ceiling or sidewall below the baggage compartment and exhausts it on the sidewall near the cabin floor. The system uses approximately 50% filtered recirculated air and 50% fresh air. During flight, the fresh air is supplied by the engine bleed air. The engine bleed air is the compressed air from the engine. The bleed air is then fed into the air conditioning system. From there, the High-Efficiency Particulate Air filter is used to remove contaminants such as dirt, dust, viruses and bacteria [1]. It is able to remove up to 99.9% of particles as small as 0.3 micrometres.

Due to the outbreak of the COVID-19, an investigation into the spreading of the virus within a confined space including an aircraft cabin has attracted researchers' attention in order to elucidate the mechanism. Passengers normally spend several hours in the cabin which makes everybody vulnerable to the infection of COVID-19. Therefore, it is crucial to investigate the spreading mechanism within the cabin which will lead to the reduction of infection in healthy passengers. However, prior to that, a study regarding the flow distribution within an aircraft cabin should be done.

Several studies investigated air distribution in aircraft cabin. Li *et al.* (2015) performed an experimental study in a single aisle seven rows seats of 737 aircraft cabin mock-up using two dimensional (2D) particle image velocimetry (PIV) [2]. Three different orientations, cross-section, horizontal and longitudinal air distribution were measured. The results showed that different cross-section airflow patterns have some similarities and random variations. A recent experimental study by Liu *et al.* (2022) measured air velocity, temperature and contaminant concentration [3]. The findings showed low air velocity and stratified air temperature in the aircraft cabin mock-up. However, the experiment was carried out in a displacement ventilation system. A study by Li *et al.* (2021) investigated the airflow, temperature, and concentrations of airborne particles in a single aisle seven row cabin mock-up with mixing ventilation system [4]. The transportation of the particles was affected by the airflow. Therefore, the understanding of the fundamental flows in aircraft cabin is essential to be performed.

The results of studies based on experiments are more reliable but they are time-consuming and expensive. According to Liu *et al.* (2013), a scale model of an aircraft cabin costs a relatively high amount of up to a million dollars or more [5] . The model may also only contain a few rows of seats. Furthermore, according to Mazumdar and Chen (2008), different conditions in the aircraft cabin would make the experimental measurement more complicated [6]. Hence, numerical modelling using a computer is preferable for studies in the aircraft cabin.

Numerical simulations using Computational Fluids Dynamics (CFD) are increasingly used in aircraft cabin. Cao *et al.* (2022) conducted a study on the effects of various aspects of airflow and particle distribution in mixing and displacement ventilation [7]. It was found that the Realizable k - ε (RLZ) model is the best turbulence model. A more recent work by Liu *et al.* (2022) investigated the performance of a displacement and mixing ventilation system in an aircraft cabin with single aisle and seven rows of seats in which the RLZ turbulence model was used in combination with the Well-Rileys model to evaluate the contaminant transmission [3]. However, the complexity of the geometry of the aircraft cabin may affect the results of the simulation.

Measuring the flow distribution in the aircraft cabin is essential to achieve high accuracy of validation. The scaled-down model is able to predict more accurate results than the complex model. CFD numerical simulation can be used to predict the flow distribution in a short time compared to the experiment. Most

previous numerical simulations used a commercial software, ANSYS; for example, the studies by Yang *et al.* (2015), You *et al.* (2019), Zhao *et al.* (2020) and Desai *et al.* (2021) [8, 9, 10,11]. However, numerical simulations with Open Source Field Operation and Manipulation (OpenFOAM) have rarely been performed in the study of aircraft cabins.

In this study, an open source software, OpenFOAM was used with three different steady Reynolds Averaged Navier-Stokes (RANS) turbulence models; Re-normalisation Group k-ε (RNG), RLZ and Low Reynold Number (LRN) to investigate the flow distribution of a scaled-down empty aircraft cabin model. The main aims of this paper are to validate the numerical simulation of CFD results with previous work of Thysen *et al.* (2022) [12] and to determine the best turbulence model to be used. The details of velocity and turbulence kinetic energy analysis are carried out to determine the characteristic of each turbulence model.

2.0 METHODOLOGY

2.1 Computational Domain

Figure 1 shows the computational domain, which is identical to the experimental setup of Thysen *et al.* (2022) [12]. The experimental setup is a generic model of an empty aircraft cabin using a scaled-down water-filled enclosure. The experimental setup is scaled-down to (1:11) with a height (H) of 200 mm, a width (W) of 300 mm, and a length (L) of 300 mm. The overhead baggage compartment in the aircraft cabin is represented by two cuboids with rounded part. The cabin has four inlets, two ceiling inlets and two side inlets. The two-opposing outlets are located at a height (t) of 20 mm from the floor.

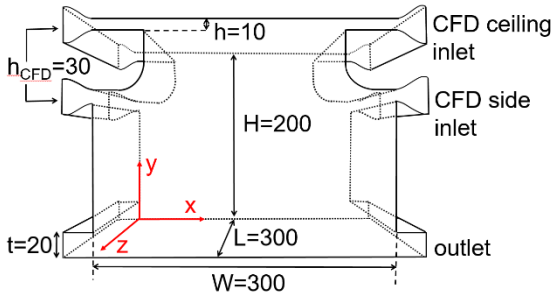

Figure 1 Computational domain (unit: mm)

The computational domain is simplified by removing the conditioning section except for the contraction region. As proposed in the experiment by Thysen *et al.* (2022) [12], the shape of the contraction region is designed based on the fifth-order polynomial of Bell and Mehta (1988) [13] and Brassard and Ferchichi (2005) [14] to reduce the velocity gradient and turbulence intensity. The height of the inlet before and after the contraction region is h_{CFD} = 30 mm and h = 10 mm, respectively. A mixing ventilation system through ceiling inlet is performed in this study. Therefore, the two-side inlet is closed as shown in Figure 2.

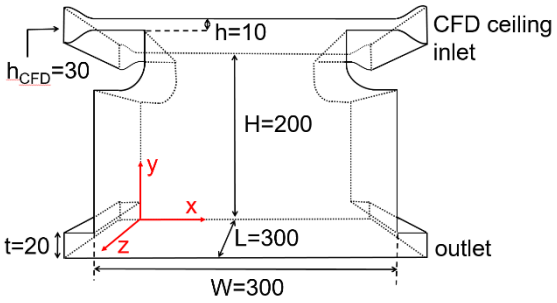

Figure 2 Computational domain for mixing ventilation (unit: mm)

2.2 Boundary Conditions

This study sets the boundary conditions as the same as in the two-dimensional (2D) Particle Image Velocimetry (PIV) experiment of Thysen *et al.* (2022) [12]. The water is supplied to the aircraft cabin through two opposing ceiling inlets on both sidewalls above the baggage compartment. The inlet velocity, 0.101 m/s is set at the height of the inlet before the contraction region, h_{CFD}. The water is discharged through the outlet on both sidewalls near the floor. The outlet is set to a zero static pressure (OpenFoam: *fixedValue uniform 0*). The turbulence intensity is set to 15 % at the inlet. The hydraulic mean diameter is calculated by measuring the length and height of the inlet, 545 mm. The wall for velocity is set to no slip condition (OpenFoam: *fixedValue uniform 0*). Furthermore, in order to have the mesh resolves near the wall, the wall function for the turbulent kinetic energy, k (OpenFOAM: *fixedValue uniform 0.000344*), the energy dissipation rate, ε (OpenFOAM: *zeroGradient*) and turbulence viscosity, nut (OpenFoam: *zeroGradient*) are applied.

2.3 Turbulence Models

In this study, two equations of three RANS turbulence models, RNG, RLZ and LRN, are used to investigate the flow fields of the scaled-down water filled aircraft cabin. The RNG model is more accurate and reliable than the standard k-ε (STD) model for a wider range of flows [15]. The RLZ model is chosen because it was used by Liu *et al.* (2022) [3] and Cao *et al.* (2022) [7] in studies of aircraft cabins. Meanwhile, the LRN model by Launder and Sharma (1974) [16] is applied to resolve the flow behaviour near the wall. All numerical simulations are solved by solving the conservation of mass equation. The equation can be written as Equation (1).

$$\nabla \cdot \vec{u} = \text{div } \mathbf{u} = 0 \quad (1)$$

where **u** is depicted as velocity vector in which the components are resolved into streamwise U, vertical V and lateral W direction, respectively. The momentum equation for each direction is written in Equation (2) ~ Equation (4).

x-direction;

$$\frac{\partial U}{\partial t}+U\frac{\partial U}{\partial x}+V\frac{\partial U}{\partial y}+W\frac{\partial U}{\partial z} = \nu\left[\frac{\partial^2 U}{\partial x^2}+\frac{\partial^2 U}{\partial y^2}+\frac{\partial^2 U}{\partial z^2}\right]-\frac{1}{\rho}\frac{\partial p}{\partial x} \quad (2)$$

y-direction;

$$\frac{\partial V}{\partial t}+U\frac{\partial V}{\partial x}+V\frac{\partial V}{\partial y}+W\frac{\partial V}{\partial z} = \nu\left[\frac{\partial^2 V}{\partial x^2}+\frac{\partial^2 V}{\partial y^2}+\frac{\partial^2 V}{\partial z^2}\right]-\frac{1}{\rho}\frac{\partial p}{\partial y} \quad (3)$$

z-direction;

$$\frac{\partial W}{\partial t}+U\frac{\partial W}{\partial x}+V\frac{\partial W}{\partial y}+W\frac{\partial W}{\partial z} = \nu\left[\frac{\partial^2 W}{\partial x^2}+\frac{\partial^2 W}{\partial y^2}+\frac{\partial^2 W}{\partial z^2}\right]-\frac{1}{\rho}\frac{\partial p}{\partial z} \quad (4)$$

where ν is the kinematic viscosity and ρ is the density of the water.

2.4 Solver Setting

An open-source software, OpenFOAM version 2106 is used to perform all the numerical simulations. Water is used as the working fluid which is considered to be Newtonian, incompressible, isothermal and constant density. The kinematic viscosity of the water is set to 1.0 x 10^{-6} m^2/s at 20 °C. Semi-Implicit Method for Pressure Linked Equations Consistent (SIMPLEC) algorithm is used to solve the governing equations through velocity and pressure coupling approach. The finite volume method is employed to discretise the governing equation. A second order linear interpolation is applied to the gradient terms while second order accurate discretization schemes are applied for the divergence and Laplacian terms. The solution is considered converged if the residuals do not decrease further with the increasing number of iterations by setting the minimum residuals to 10^{-5} pressure, turbulent kinetic energy and turbulence dissipation rate. The simulations are performed at Wind Engineering and Building Physics Center (WEBPC) of Universiti Teknologi MARA using 12 processors consisting of 2 × 6-core Intel Xeon E5-2620 v3 CPU @ 2.4 GHz.

2.5 CFD Validation

A quantitative comparison between the CFD numerical simulation and experimental results is performed using three validation metrics to evaluate the performance of the CFD, the factor of two of observations (FAC2), root mean square error (RMSE) and the normalized mean square errors (NMSE). The three validation metric equations, FAC2 (Equation 5), RMSE (Equation 6) and NMSE (Equation 7) can be described as follows:

$$\mathrm{FAC2}=\frac{1}{N}\sum_{i=1}^{N} n_i \text{ with } n_i=\begin{cases} 1 \text{ for } 0.5 \ll \frac{P_i}{O_i} \ll 2 \\ 0 \text{ else} \end{cases} \quad (5)$$

$$\mathrm{RMSE}=\sqrt{\frac{\sum_{i=1}^{n}(P_i-O_i)^2}{\sum_{i=1}^{n}{O_i}^2}} \quad (6)$$

$$\mathrm{NMSE}=\frac{[(O_i-P_i)^2]}{[O_i][P_i]} \quad (7)$$

where P_i and O_i represent CFD numerical simulation data and experimental data, respectively. The square brackets denote the averaging over the whole data. It should be noted that NMSE cannot be used when the value of both velocity is positive and negative.

3.0 RESULTS AND DISCUSSION

3.1 Grid Sensitivity

A grid sensitivity analysis was performed for the RNG model over three different grid sizes. The grid numbers of 6 023 119 (coarse), 12 807 257 (medium), and 17 400 893 (fine) were constructed as shown in Figure 3. The mesh was generated by *snappyHexMesh* utility in the OpenFOAM software.

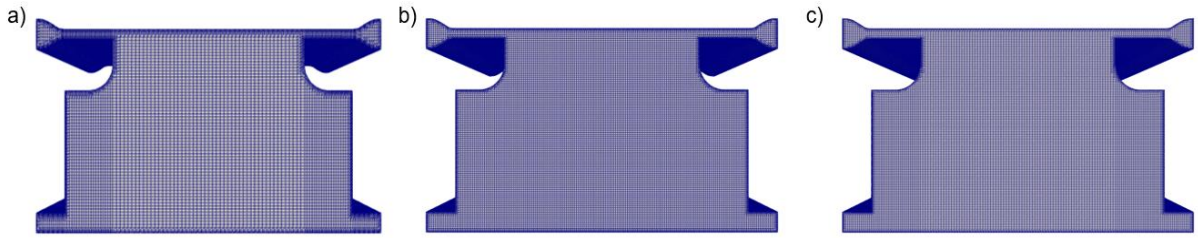

Figure 3 Mesh resolution for grid sensitivity analysis (a) coarse grid: 6 023 119 (b) medium grid: 12 807 257 (c) fine grid: 17 400 893

Figure 4 shows the normalised mean x-velocity profile, U/U_{max} for three different grids, coarse, medium, and fine. U is the mean x-velocity and U_{max} is the maximum velocity at the inlet. The non-dimensional distance y+ ≈ 7 is for coarse grid and y+ ≈ 5 is for medium and fine grids. The profile is measured at five vertical lines of x/H = 0.13, 0.38, 0.75, 1.12, and 1.37 in the middle of x-y plane (z/H = 0.75) of the aircraft cabin. The coarse grid, medium grid and fine grid are nearly identical at all five vertical lines which is close to the experiment data by Thysen *et al.* (2022) [12] except at near the inlet region or jet region (y/H > 0.9) and near the outlet region (y/H < 0.2).

All grid models overestimate the jet region which is consistent with the simulation results of Thysen *et al.* (2021) [17]. Another discrepancy is observed at the region near the floor (y/H < 0.2) which also agrees with the results of Thysen *et al.* (2021) [17]. Therefore, all grid models can be used for the numerical simulation. However, since the y+ for the coarse grid is approximately equal to 7 , the medium grid with y+ ≈ 5 is used to calculate the Grid Convergence Index (GCI). This choice is to ensure the selected mesh is sufficient enough to resolve near the wall flow.

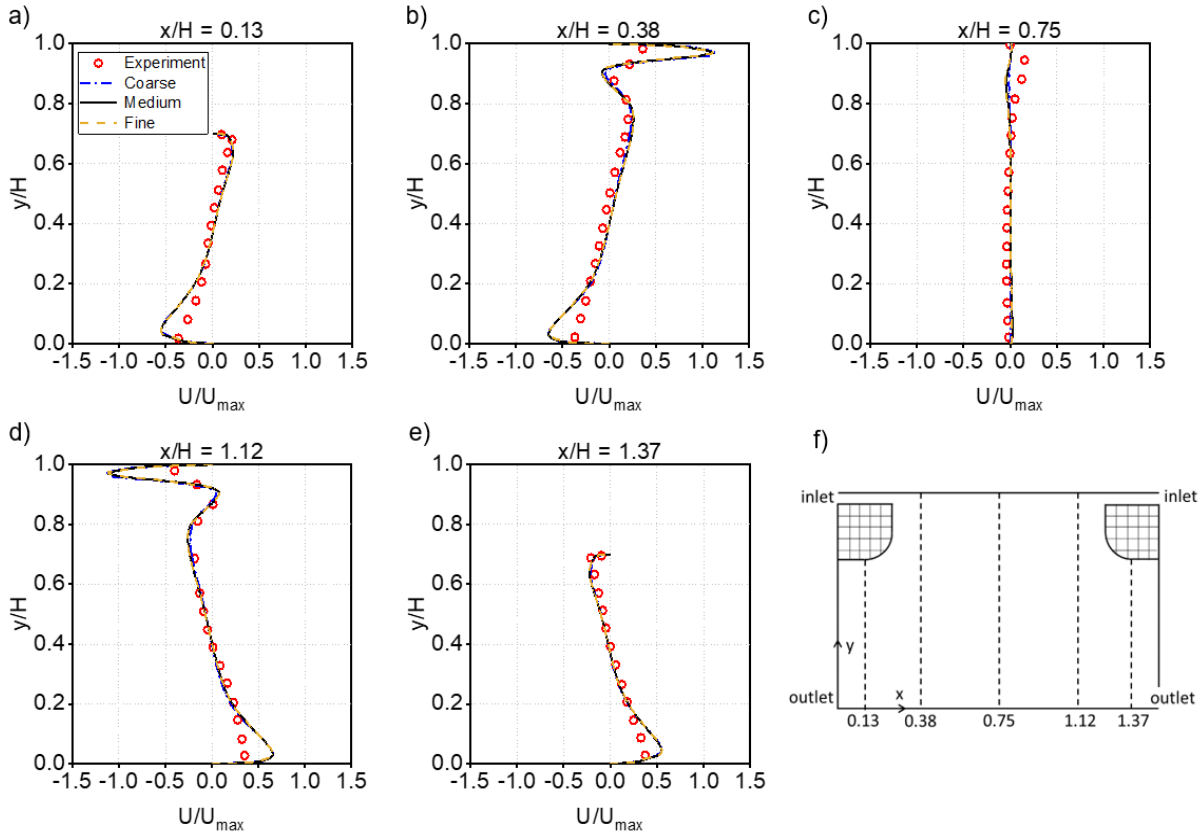

Figure 4 Grid sensitivity analysis on normalised mean x-velocity profile, U/Umax at x/H = 0.13 (b) x/H = 0.38 (c) x/H = 0.75 (d) x/H = 1.12 (e) x/H = 1.37 as shown in (f). Coarse: blue dash dot line; medium: black solid line; and fine: orange dash line

Figure 5 presents the GCI for medium grids to quantitatively estimate the error of the medium grid towards fine grid at the five vertical lines. The error bars represent the GCI value as proposed by Roache (1997) [18] which can be written as Eq. 8:

$$\mathrm{GCI_{medium}} = \mathrm{F_S}\left|\mathrm{r^p}\frac{[(\mathrm{U/U})_{\mathrm{medium}} - (\mathrm{U/U_{max}})_{\mathrm{fine}}]}{\mathrm{r^p}-1}\right| \quad (8)$$

where Fs, r and p are safety factor, linear grid refinement factor and formal order of accuracy, respectively. In this study, the Fs value is 1.25, considering the use of coarse, medium and fine grids. The r is 1.33 which is the refinement factor of fine mesh to medium mesh. p is 2 since the second order of accuracy is employed in the simulation. The average value of the GCI for five vertical lines is in the range of 1% to 2.19%. The medium grid shows grid independent; therefore, it is fine enough to be employed for the rest of the numerical simulation in this study.

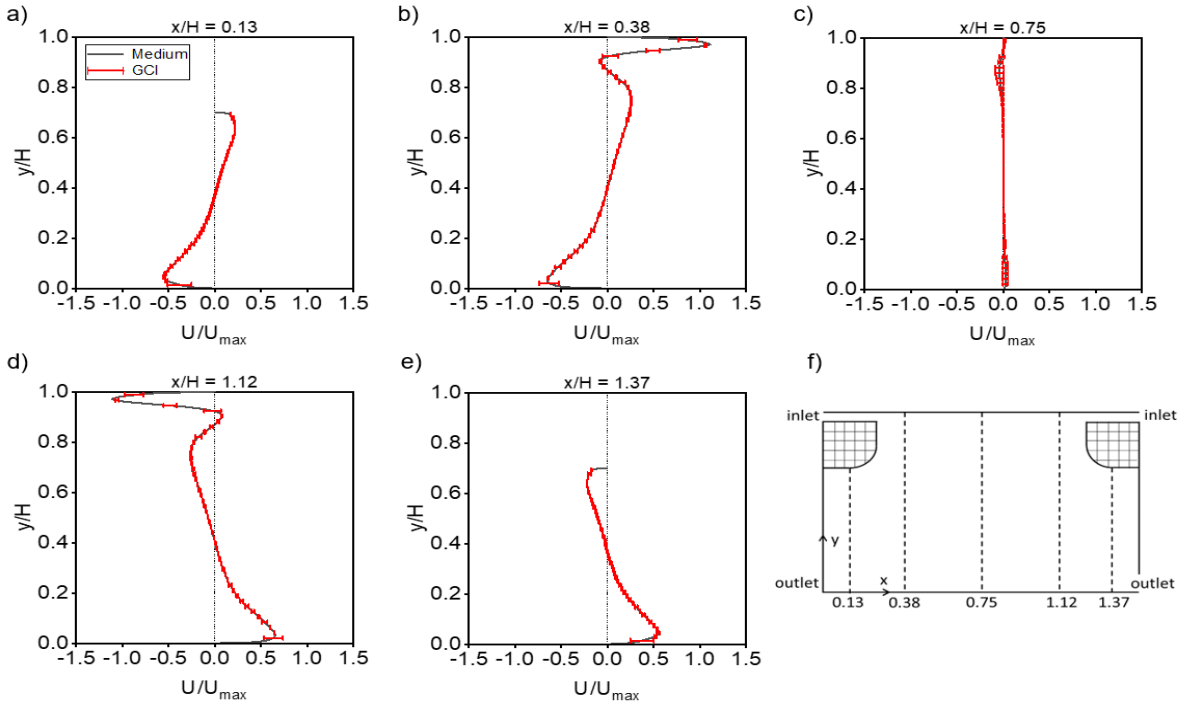

Figure 5 GCI on normalised mean x-velocity profile, U/U_{max} (a) x/H = 0.13 (b) x/H = 0.38 (c) x/H = 0.75 (d) x/H = 1.12 (e) x/H = 1.37 as shown in (f). Medium grid: black solid line, GCI: error bar

3.2 Normalised Velocity Vector and Contour

Figure 6 depicts the normalised velocity vector and contour for the RNG, RLZ and LRN models at the middle of x-y plane (z/H = 0.75). The flow exits from the two opposite inlets above the baggage compartment which collides each other at the middle of the cabin and changes its direction towards the floor. Near the floor, the flow is separated into two that move towards the outlets. Most of the flow is discharged at the two outlets near the floor and the rest flows back upwards. As a result, a fairly symmetrical circulation flow can be seen on the right and left sides of the aircraft cabin model, representing the passenger area in the cases of the RNG and LRN turbulence models. This is indicative of a study by Zhang *et al.* (2017) [19]. Considering this circulation, the flow could affect the spread of the virus if one of the passengers is unhealthy. Therefore, further studies on the efficiency of ventilation and the spread of pollutants or viruses are needed.

A high velocity is observed near the inlet and outlet region. Distances from these flow regions result in a lower air velocity [20]. Therefore, a lower velocity is observed at other region. However, high velocity is observed in the centre of the aircraft cabin model where the opposing flow from the two ceiling inlets merges.

Meanwhile, for the RLZ turbulence model, an asymmetric pattern is observed. The contour shows asymmetric circulation on the left and right side of the cabin. This can also be observed in the next section where the RLZ model fails to accurately predict the velocity and turbulence kinetic energy.

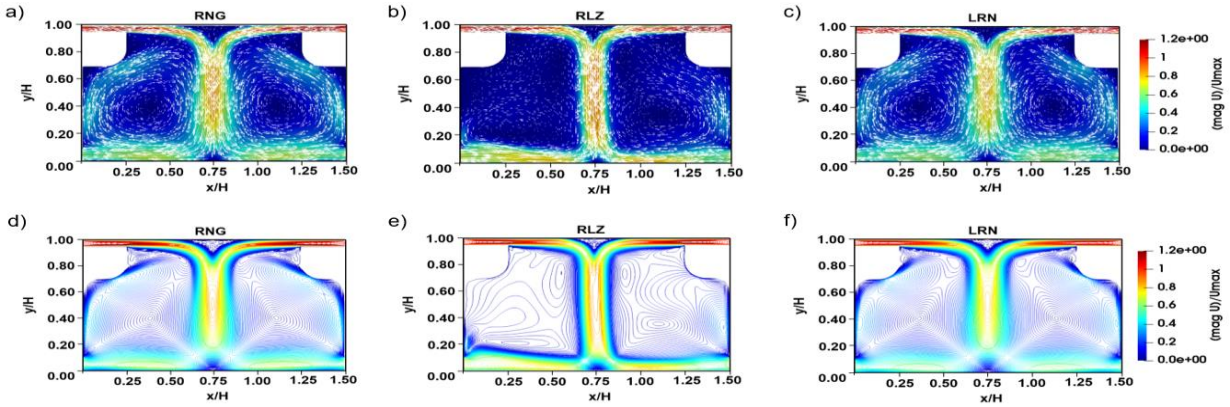

Figure 6 Normalised velocity vector and contour of magnitude of velocity, U at z/H = 0.75 (a) RNG turbulence model (b) RLZ turbulence model and (c) LRN turbulence model

3.3 Profiles and Validation

Figure 7 (a-e) presents the vertical profiles of the normalised mean x-velocity, U/U_{max} at five vertical lines, x/H = 0.13, 0.38, 0.75,1.12 and 1.37 of mid x-y plane (z/H = 0.75). At x/H = 0.13 and x/H = 1.37, the RNG model and the LRN model show fairly good agreement except near the outlet region (y/H < 0.2). This could be due to the resolution of the measurement. At x/H = 0.38 and x/H = 1.12, a slight deviation is observed near the inlet region (y/H > 0.9), which is due to the influence of the inlet jet flow. At x/H = 0.75, both models are slightly underestimated at near the inlet region (y/H > 0.9).

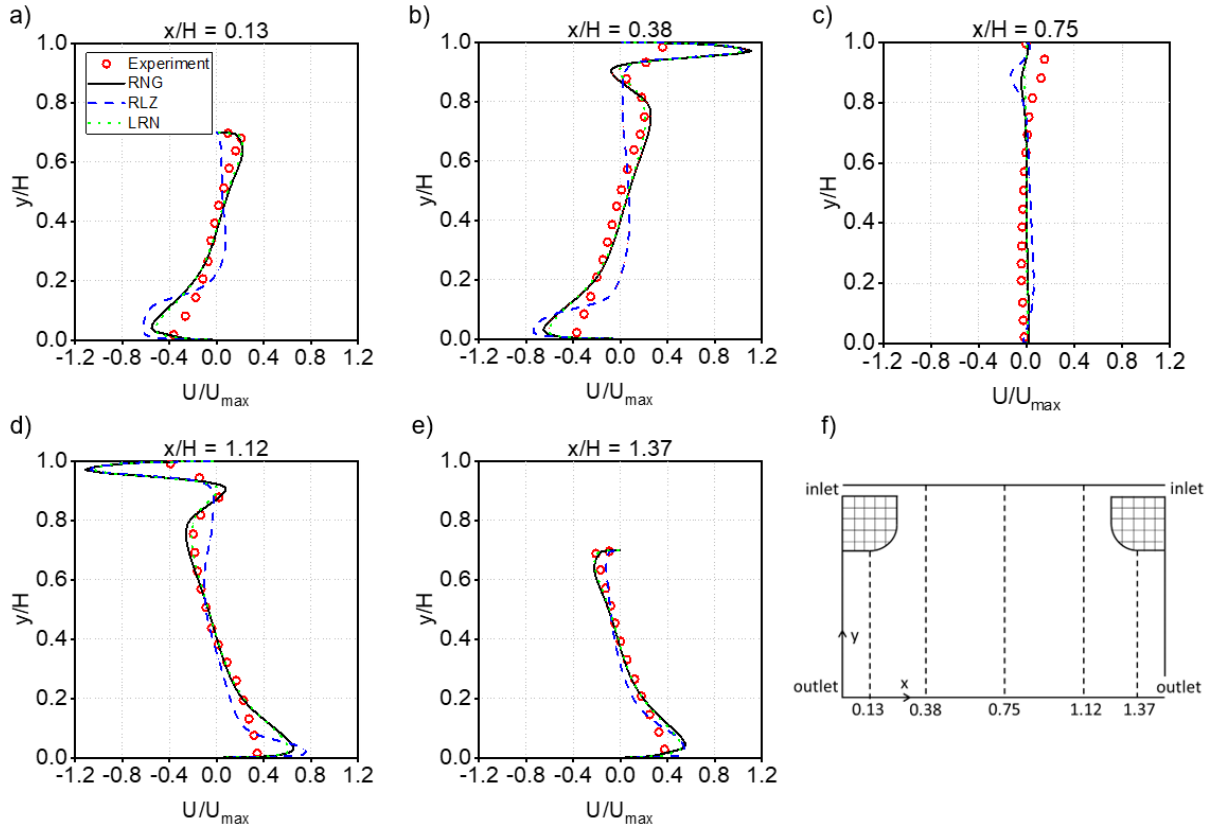

Figure 7 (a - e): Normalised mean x-velocity profile, U/U_{max} at five vertical lines at z/H = 0.75 as shown in (f). Experiment: red circle, RNG: black solid line, RLZ: blue dash line, LRN: green dot line

Quantitatively, as shown in Table 1, the value of FAC2 is the same for both turbulence models, 0.65 which is approximately similar to previous study [17]. The RMSE value for both of the RNG model and the LRN model is 0.07, which is slightly better. For the RLZ model, it obviously deviates from the experimental result at almost location especially at x/H = 0.13, 0.38 and 1.12. The value of FAC2 and RMSE is higher than the RNG and LRN models compared to the ideal value, 0.33 and 0.10, respectively. At x/H = 0.75, the RLZ model is underestimated at the centre of the cabin model as both inlets flow into the merging region.

Table 1 Validation Metrics for U/U_{max}

Turbulence Model	U/U_{max}		U/U_{max} [19]	
	FAC2	RMSE	FAC2	RMSE
RNG	0.65	0.07	0.64	0.08
RLZ	0.33	0.10	-	-
LRN	0.65	0.07	0.64	0.08

For the normalised mean y-velocity profile, V/U_{max} as shown in Figure 8 (a-e), all models predict stronger downward flow at the middle position (x/H = 0.75) where the opposing flows merge. At x/H = 0.38, 1.12 and 1.37, all models depict fairly good agreement with the experimental results, even though the RLZ model shows a slight underestimation in some locations compared to the RNG and LRN models. At x/H = 0.13, the RLZ model obviously underestimates, while the RNG model and the LRN model show good agreement with the experimental result. In addition, as shown in Table 2, the FAC2 and RMSE values for RNG model and LRN model show better evaluation than previous work [17].

Table 2 Validation Metrics for V/U_{max}

Turbulence Model	V/U_{max}		V/U_{max} [17]	
	FAC2	RMSE	FAC2	RMSE
RNG	0.56	0.08	0.65	0.11
RLZ	0.33	0.10	-	-
LRN	0.56	0.07	0.61	0.13

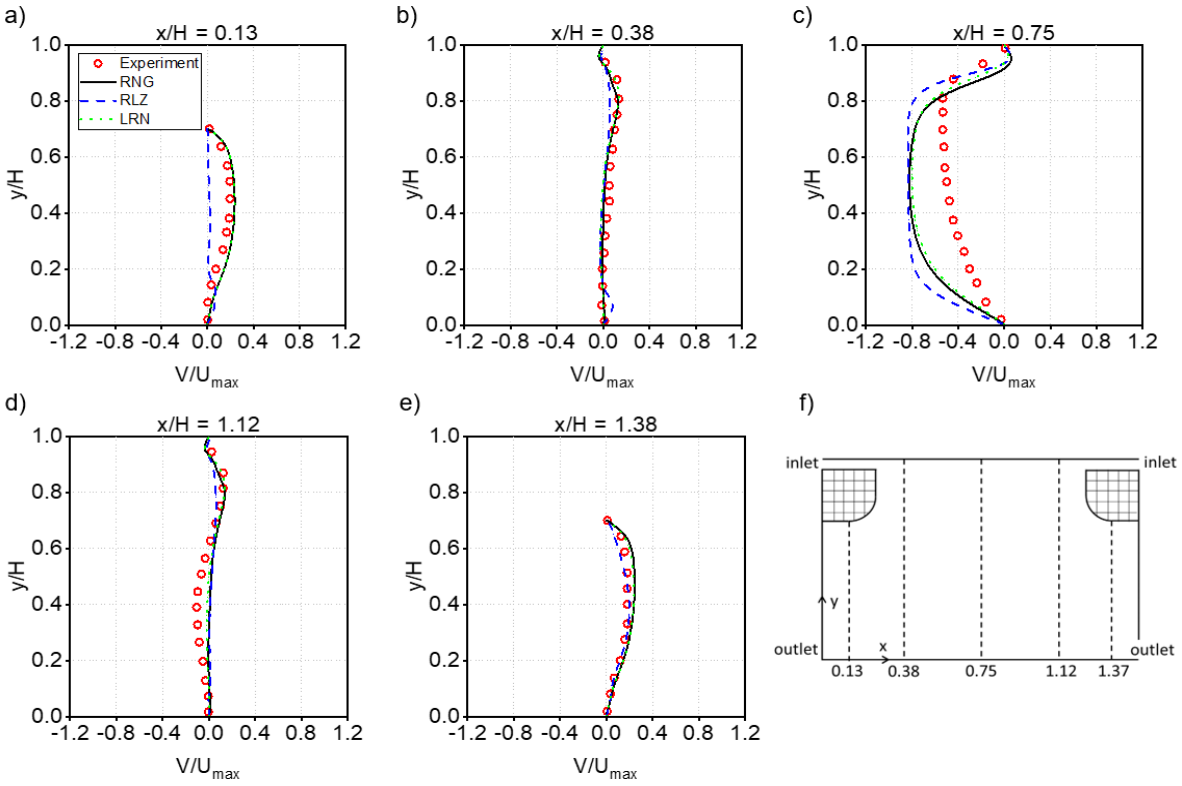

Figure 8 (a - e): Normalised mean y-velocity profile, V/U_{max} at five vertical lines at z/H = 0.75 as shown in f). Experiment: red circle, RNG: black solid line, RLZ: blue dash line, LRN: green dot line

Figure 9 (a-e) shows the normalised profile of turbulent kinetic energy, k/U_{max}^2 at five vertical lines, x/H = 0.13, 0.38, 0.75, 1.12 and 1.37. The measurement is taken at the middle of x-y plane (z/H = 0.75). The RLZ model deviates significantly from the experimental result for all five vertical lines. However, these results are consistent with the simulation of Thysen *et al.* (2021) [17].

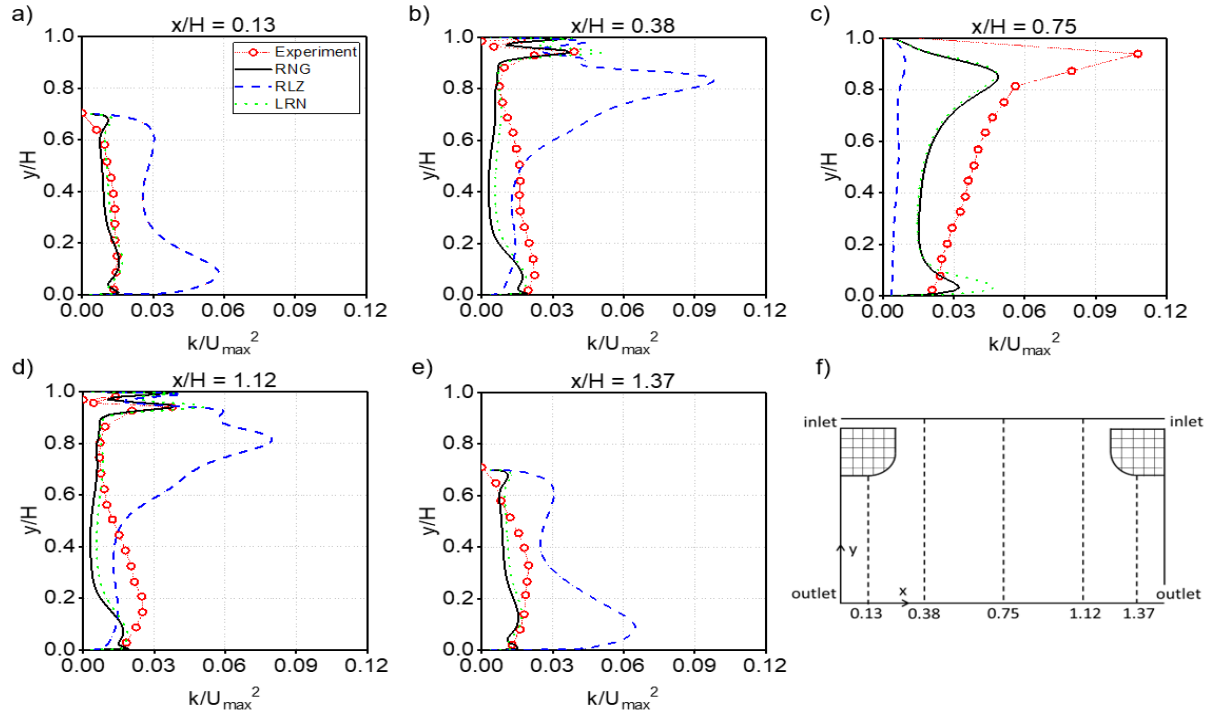

Figure 9 (a - e): Normalised TKE profile, k/Umax2 at five vertical lines at z/H = 0.75 as shown in (f) Experiment: red circle, RNG: black solid line, RLZ: blue dash line, LRN: green dot line

As shown in Table 3, the FAC2 and NMSE values represent the unacceptable value. The RNG and the LRN models also fall short of predictions at most locations. However, from the quantitative comparison using validation metrics, it can be concluded that the LRN model gives a better prediction compared to the RNG model. The RLZ model, on the other hand, shows the worst performance of all. This can also be seen in Figure 10, where most of the results of the RLZ turbulence model are in the range of above 50 % or below -50 % when compared to the experimental results. All these results may be due to the sensitivity of the turbulent kinetic energy to the resolution of the mesh.

Table 3 Validation Metrics for k/U_{max}^2

Turbulence Model	k/U_{max}^2		k/U_{max}^2 [17]	
	FAC2	NMSE	FAC2	NMSE
RNG	0.59	0.62	0.65	0.68
RLZ	0.35	2.21	-	-
LRN	0.64	0.40	0.73	0.64

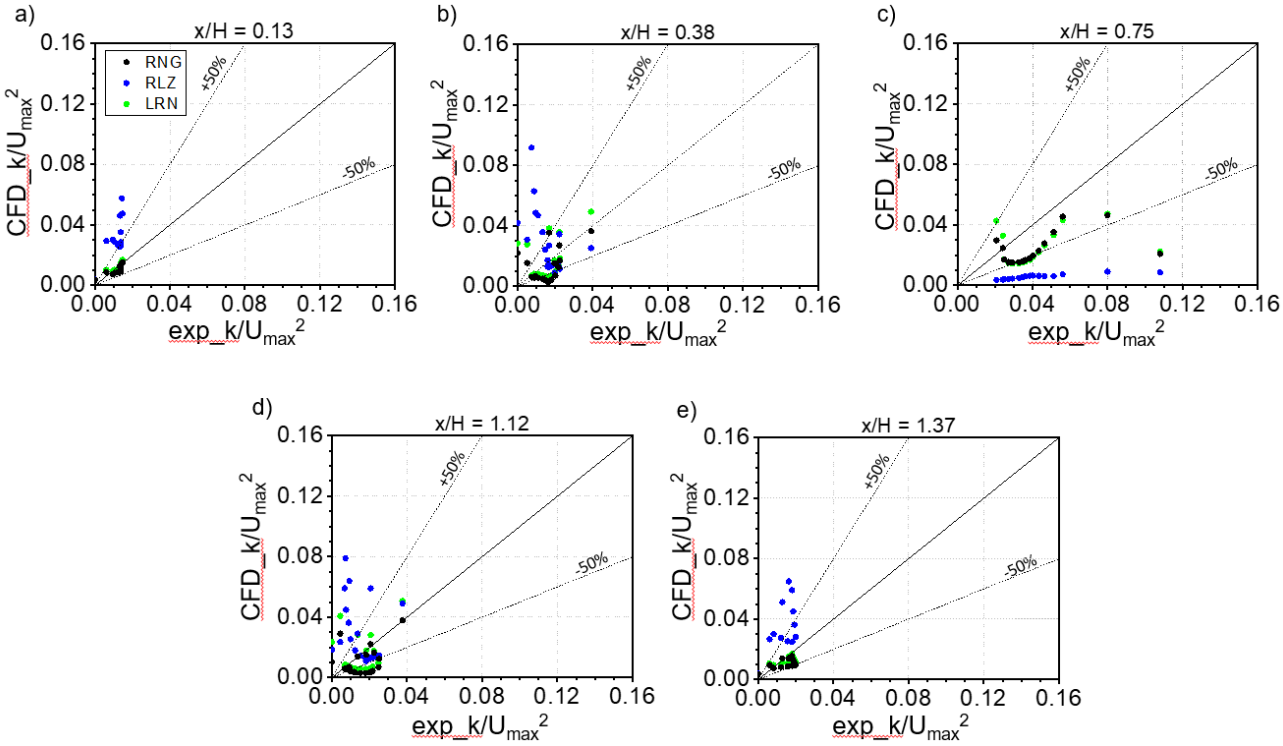

Figure 10 Scatter plots of CFD measurement with experimental measurement

4.0 CONCLUSION

We performed CFD numerical simulations with the open-source software, OpenFOAM using two equations of RANS turbulence models, the LRN, RNG and RLZ models, to investigate the flow distribution in a scaled-down model of an empty aircraft cabin with mixing ventilation system. In the RNG and LRN turbulence models, large circulation flows were observed at both sides of the aircraft cabin model, i.e. in the passenger area. The grid sensitivity analysis shows that a medium grid of 12 807 257 meshes is appropriate for numerical simulation. The GCI also indicates an acceptable value. For validation purposes, we compared the results with previous work in the literature. The RNG and LRN turbulence models agreed well with the results of previous studies while the RLZ model showed significant deviation compared to the other models. In addition, the LRN turbulence model overcome other models in predicting the mean x and y velocities and turbulent kinetic energy based on the quantitative evaluation of FAC2, RMSE and NMSE. To conclude, the CFD numerical simulation with OpenFOAM is sufficiently reproduced the flow distribution in a scaled-down empty aircraft cabin.

Conflicts of Interest

The author(s) declare(s) that there is no conflict of interest regarding the publication of this paper.

Acknowledgement

We would like to acknowledge the support provided by Universiti Kuala Lumpur to the first author in her work as a PhD student at the School of Mechanical Engineering, College of Engineering, Universiti

Teknologi MARA, (UiTM) Shah Alam. Our sincere thanks also go to the Wind Engineering & Building Physics Centre (WEBPC), UiTM Shah Alam for providing the necessary resources and facilities.

References

[1] 2019. ASHRAE Handbook: HVAC Applications-Chapter 13-Aircraft. Atlanta: ASHRAE.
[2] Li, J., Cao, X., Liu, J., Wang, C. and Zhang, Y. 2015. Global Airflow Field Distribution in a Cabin Mock-up Measured Via Large-scale 2D-PIV. *Building and Environment*. 93: 234-244. Doi: https://doi.org/10.1016/j.buildenv.2015.06.030.
[3] Liu, M., Liu, J., Cao, Q., Li, X., Liu, S., Ji, S., Lin, C.H., Wei, D., Shen, X., Long, Z. and Chen, Q. 2022. Evaluation of Different Air Distribution Systems in a Commercial Airliner Cabin in Terms of Comfort and COVID-19 Infection Risk. *Building and Environment*. 208: 108590. Doi: https://doi.org/10.1016/j.buildenv.2021.108590.
[4] Li, X., Zhang, T. T., Fan, M., Liu, M., Chang, D., Wei, Z. D., Lin, C. H., Ji, S., Liu, J., Shen, S. and Long, Z. 2021. Experimental Evaluation of Particle Exposure at Different Seats in a Single-aisle Aircraft Cabin. *Building and Environment*. 202: 108049. Doi: https://doi.org/10.1016/j.buildenv.2021.108049.
[5] Liu, W., Wen, J., Lin, C.H., Liu, J., Long, Z. and Chen, Q. 2013. Evaluation of Various Categories of Turbulence Models for Predicting Air Distribution in an Airliner Cabin. *Building and Environment*. 65: 118-131. Doi: https://doi.org/10.1016/j.buildenv.2013.03.018.
[6] Mazumdar, S. and Chen, Q. 2008. Influence of Cabin Conditions on Placement and Response of Contaminant Detection Sensors in a Commercial Aircraft. *Journal of Environmental Monitoring*. 10(1): 71-81. Doi: https://doi.org/10.1039/b713187a.
[7] Cao, Q., Liu, M., Li, X., Lin, C.H., Wei, D., Ji, S., Zhang, T. T. and Chen, Q. 2022. Influencing Factors in the Simulation of Airflow and Particle Transportation in Aircraft Cabins by CFD. *Building and Environment*. 207: 108413. Doi: https://doi.org/10.1016/j.buildenv.2021.108413.
[8] Yang, C., Zhang, X., Cao, X., Liu, J. and He, F. 2015. Numerical Simulations of the Instantaneous Flow Fields in a Generic Aircraft Cabin with Various Categories Turbulence Models. *Procedia Engineering*. 121: 1827-1835. Doi: https://doi.org/10.1016/j.buildenv.2015.10.022.
[9] You, R., Lin, C. H., Wei, D. and Chen, Q. 2019. Evaluating the Commercial Airliner Cabin Environment with Different Air Distribution Systems. *Indoor Air*. 29(5): 840-853. Doi: https://doi.org/10.1111/ina.12578.
[10] Zhao, Y., Liu, Z., Li, X., Zhao, M. and Liu, Y. 2020, June. A Modified Turbulence Model for Simulating Airflow Aircraft Cabin Environment with Mixed Convection. *Building Simulation*. 13(3): 665-675. Doi: https://doi.org/10.1007/s12273-020-0609-2.
[11] Desai, P. S., Sawant, N. and Keene, A. 2021, December. On COVID-19-safety Ranking of Seats in Intercontinental Commercial Aircrafts: A Preliminary Multiphysics Computational Perspective. *Building Simulation*. 14(6): 1585-1596. Doi: https://doi.org/10.1007/s12273-021-0774-y.
[12] Thysen, J. H., van Hooff, T., Blocken, B. and van Heijst, G. 2022. PIV Measurements of Opposing-jet Ventilation Flow in a Reduced-scale Simplified Empty Airplane Cabin. *European Journal of Mechanics-B/Fluids*. 94: 212-227. Doi: https://doi.org/10.1016/j.euromechflu.2022.03.001.
[13] Bell, J. H. and Mehta, R. D. 1988. *Contraction Design for Small Low-speed Wind Tunnels* (No. NASA-CR-177488). Doi: https://ntrs.nasa.gov/citations/19890004382.
[14] Brassard, D. and Ferchichi, M. 2005. Transformation of a Polynomial for a Contraction Wall Profile. *J. Fluids Eng.* 127(1): 183-185. Doi: https://doi.org/10.1115/1.1852492.
[15] Li, M., Yan, Y., Zhao, B., Tu, J., Liu, J., Li, F. and Wang, C. 2018. Assessment of Turbulence Models and Air Supply Opening Models for CFD Modelling of Airflow and Gaseous Contaminant Distributions in Aircraft Cabins. *Indoor and Built Environment*. 27(5): 606-621. Doi: https://doi.org/10.1177/1420326X16688049.
[16] Launder, B. E. and Sharma, B. I. 1974. Application of the Energy-dissipation Model of Turbulence to the Calculation of Flow Near a Spinning Disc. *Letters in Heat and Mass Transfer*. 1(2): 131-137. Doi: https://doi.org/10.1016/0094-4548(74)90150-7.
[17] Thysen, J. H., van Hooff, T., Blocken, B. and van Heijst, G. J. F. 2021. CFD Simulations of Two Opposing Plane Wall Jets in a Generic Empty Airplane Cabin: Comparison of RANS and LES. *Building and Environment*. 205: 108174. Doi: https://doi.org/10.1016/j.buildenv.2021.108174.
[18] Roache, P. J. 1997. Quantification of Uncertainty in Computational Fluid Dynamics. *Annual Review of Fluid Mechanics*. 29(1): 123-160. Doi: https://doi.org/10.1146/annurev.fluid.29.1.123.
[19] Zhang, Y., Liu, J., Pei, J., Li, J. and Wang, C. 2017. Performance Evaluation of Different Air Distribution Systems in an Aircraft Cabin Mockup. *Aerospace Science and Technology*. 70: 359-366. Doi: https://doi.org/10.1016/j.ast.2017.08.009.
[20] W. F. M. 2020. The Effects of Various Opening Sizes and Configurations to Air Flow Dispersion and Velocity in Cross-ventilated Building. *Jurnal Teknologi*. 82(4). Doi: https://doi.org/10.11113/jt.v82.14537.